Optik - International Journal for Light and Electron Optics 233 (2021) 166613

Contents lists available at ScienceDirect

Optik

journal homepage: www.elsevier.com/locate/ijleo

Original research article

Propagation of hyperbolic sinusoidal Gaussian beams in uniaxial crystals orthogonal to the optical axis

Mert Bayraktar

Hasan Kalyoncu University, Department of Electric Electronic Engineering, Havaalanı Yolu 8. Km, Şahinbey, Gaziantep, 27410, Turkey

ARTICLE INFO

Keywords:
Hyperbolic sinusoidal Gaussian beam
Uniaxial crystal
Propagation

ABSTRACT

In this paper, hyperbolic sinusoidal Gaussian(HSG) beam propagates in uniaxial crystal orthogonal to the propagation axis. Received field expression is evaluated analytically based upon Huygens-Fresnel integration. Numerical results are plotted in order to analyze the effect of variations in source beam parameters, crystal refractive index features, and propagation distance. We investigate that beam size and peak intensity of received beam can be managed by adjusting crystal structure. We anticipate that our results will be useful for optical tracking applications.

1. Introduction

In recent years, applications on crystals arouse interest of scientists. It is the first time to derive exact formula for the reflection and refraction coefficients in crystal [1]. Previous method is improved and a 2×2 matrix method is used in order to find reflection coefficients [2]. Then, crystal properties are derived using four reflection coefficients [3]. Next, analytical expression of optical coefficients is derived in case of an isotropic layer is placed on a uniaxial crystal [4]. In addition to reflection coefficients, transmission coefficients are given for anisotropic uniaxial crystal [5]. Considering the bounds of reflection in crystal, Brewster angle, which is the angle where incident ray passes directly without reflection, formula is given when crystal is placed on optical axis [6]. By taking into consideration Brewster angle, it is found in [7] that one of the reflection amplitudes becomes zero when refractive index of incident medium is in between ordinary and extraordinary refractive indexes. Later on, relationship between polarizing angle and Brewster angle is given [8].

In other point of view, generation or propagation of untraditional beams benefiting from uniaxial crystals are studied in the literature. It is shown in [9] that Bessel vortices can be generated using photonic crystals. Moreover, beams having fractional optical vortices can be generated with 95 % energy efficiency using uniaxial crystal [10]. Experimental generation of Full Poincare beam using uniaxial crystal is presented [11]. Another experimental set-up is established in [12] and it is resulted as Gaussian beam focuses at a close distance. Polarization modulation is applied to the vector beams experimentally using crystals [13]. In another point of view, nonconventional beams are used in the input of the uniaxial crystals. Accordingly, Olver function, which is evaluated as integrating an complex exponential, is used to obtain Olver Gaussian beam and it is indicated that finite Olver Gaussian beam has asymmetric intensity profile for extraordinary refractive index is less than ordinary refractive index [14]. Likely, random electromagnetic

E-mail address: mert.bayraktar@hku.edu.tr.

https://doi.org/10.1016/j.ijleo.2021.166613
Received 8 January 2021; Received in revised form 2 February 2021; Accepted 21 February 2021
Available online 23 February 2021

multi-Gaussian Schell-model vortex beams also turn into elliptical shape [15]. In addition, four-petal Lorentz-Gauss beam and partially coherent Lorentz-Gauss beam have elliptic distribution after long distance propagation in uniaxial crystal [16–18]. In addition to elliptic shape, rectangular multi-Gaussian Schell-model vortex beam gains flat-topped profile [19]. Oppositely, elliptical Gaussian beam becomes symmetric in long distance [20]. It is possible to see four petal view at the output of the crystal by adjusting the refractive indexes if Hermite-cosine-Gaussian beam is applied from the input [21]. Strength of self-bending effect reduces if the ratio of extraordinary refractive index to ordinary refractive index goes up [22]. Distance which maximum intensity observed has an inverse relationship with the ratios of refractive indexes [23]. Beam size of cosh-Airy beam is larger as compared to Airy beam as it is indicated in [24]. Intensity of off-axis hollow vortex Gaussian beam turns during the long propagation in crystal [25]. Lastly, maximum gradient force of radially polarized Pearcey beam propagating in uniaxial crystal is found in the side lobes [26]. Variation in initial angle shifts the radially polarized Airy-Gaussian beam to off axis [27]. In addition, acceleration of Airy-Gaussian vortex beam lose strength when distribution factor increases [28]. Effect of first order chirped factor is more in x-direction than y-direction for radially polarized chirped Airy beam [29]. Furthermore, angular momentum of chirped Airy vortex beam changes with chirped factor [30]. Chirped factor can control rotation velocity of rotating elliptical chirped Gaussian beam [31]. Lastly, Airyprime beam evolves into flat topped shape after propagation through uniaxial crystal [32].

In this article, we derive the received field of astigmatic hyperbolic sinusoidal Gaussian beam propagating in uniaxial crystal orthogonal to the optical axis. Received field expression is found based on Huygens-Fresnel integral. Numerical results are plotted considering the variations in source beam parameters, ratio of extraordinary refractive index to ordinary refractive index, and propagation distance. In the rest of the paper, analytical derivation is presented in Section 2. Comments on numerical results are located in Section 3 and concluding remarks are seen in Section 4.

2. Derivation of received field in uniaxial crystal

Source field expression of HSG beam is written as [33]

$$u_s(s_x, s_y) = sinh(as_x)sinh(bs_y)exp\left(-\frac{s_x^2 + s_y^2}{w^2}\right) \tag{1}$$

where (s_x, s_y) refer to transverse source plane coordinates, w stands for Gaussian beam size, a and b correspond to argument of hyperbolic sinusoidal function. Here, it is also known that hyperbolic sinusoidal function can be expressed in terms of exponential functions as

$$sinh(x) = \frac{\exp(x) - \exp(-x)}{2} \tag{2}$$

After re-arranging Eqs. (1) and (2), source field expression is re-written as

$$u_s(s_x, s_y) = \frac{1}{4}\begin{pmatrix} \exp(as_x + bs_y) - \exp(as_x - bs_y) \\ -\exp(-as_x + bs_y) + exp(-as_x - bs_y) \end{pmatrix} exp\left(-\frac{s_x^2 + s_y^2}{w^2}\right) \tag{3}$$

In other point of view, we write relative di-electric tensor of uniaxial crystal from [34] as

$$\varepsilon = \begin{pmatrix} n_e^2 & 0 & 0 \\ 0 & n_0^2 & 0 \\ 0 & 0 & n_0^2 \end{pmatrix} \tag{4}$$

where n_e and n_0 are known as extraordinary and ordinary refractive indexes of crystal. We define the ratio $e = n_e/n_0$ and n_0 is set to 2.62. Benefiting from Huygens-Fresnel integral, received field expression in uniaxial crystal is written [35] in Eq. (5) as

$$u_r(r_x, r_y) = \frac{kn_0}{2\pi jz} exp(-jkn_e z) \int_{-\infty}^{\infty}\int_{-\infty}^{\infty} ds_x ds_y u_s(s_x, s_y) \\ xexp\left(\frac{jk}{2zn_e}\left[n_0^2(r_x - s_x)^2 + n_e^2(r_y - s_y)^2\right]\right) \tag{5}$$

Here, (r_x, r_y) indicate receiver plane coordinates and z refers to propagation distance. Propagation distance is determined based on Rayleigh distance. Rayleigh distance is found as $z_R = kw^2$. Here, k is being the wave number and it is evaluated as $2\pi/\lambda$. Operating wavelength λ is set to $0.53\mu m$ in this study. Source field expression in Eq. (3) is composed of sum of four exponential functions. Because

of this reason, received field will involve four parts named as u_{r1}, u_{r2}, u_{r3}, and u_{r4}. In the light of these, general expression for received field is written in Eq. (6) as

$$u_r(r_x, r_y) = \frac{kn_0}{4\pi jz} exp(jkn_e z)\left(u_{r1}(r_x, r_y) + u_{r2}(r_x, r_y) + u_{r3}(r_x, r_y) + u_{r4}(r_x, r_y)\right) \tag{6}$$

By substituting the first part of source field expression in Eq. (3) into Eq. (5), we have

$$u_{r1}(r_x, r_y) = \int_{-\infty}^{\infty}\int_{-\infty}^{\infty}\left(exp(as_x + bs_y) exp\left(-\frac{s_x^2 + s_y^2}{w^2}\right) exp\left(\frac{jk}{2zn_e}\left[n_0^2(r_x - s_x)^2 + n_e^2(r_y - s_y)^2\right]\right) ds_x ds_y\right) \tag{7}$$

Re-organized form of Eq. (7) gives us

$$u_{r1}(r_x, r_y) = \int_{-\infty}^{\infty}\int_{-\infty}^{\infty}\left(exp(as_x + bs_y) exp\left(-\frac{s_x^2 + s_y^2}{w^2}\right) exp\left(\frac{jk}{2zn_e}\left[\begin{array}{c} n_0^2(r_x^2 - 2r_x s_x + s_x^2) \\ +n_e^2(r_y^2 - 2r_y s_y + s_y^2) \end{array}\right]\right) ds_x ds_y\right) \tag{8}$$

To see the general view of Eq. 8, we define new variables as in Eq. (9) below.

$$\begin{aligned} p_x &= \frac{jkw^2 n_0^2 - 2zn_e}{2zn_e\omega^2} \\ q_{x1} &= -\frac{jkn_0^2 r_x}{zn_e} + a \\ p_y &= \frac{jkw^2 n_e - 2z}{2z\omega^2} \\ q_{y1} &= -\frac{jkn_e r_y}{z} + b \\ q_{x2} &= -\frac{jkn_0^2 r_x}{zn_e} - a \\ q_{y2} &= -\frac{jkn_e r_y}{z} - b \end{aligned} \tag{9}$$

Here, p_x and p_y are the coefficients for the terms s_x^2 and s_y^2 respectively. q_{x1}, q_{x2}, q_{y1}, and q_{y2} are the coefficients which will be selected for s_x and s_y according to the evaluated part of the received field. Using the new defined variables above, general expression of first component of received field is written as

$$\begin{aligned} u_{r1}(r_x, r_y) &= exp\left(\frac{jkn_0^2}{2zn_e} r_x^2 + \frac{jkn_e}{2z} r_y^2\right) \\ x &\int_{-\infty}^{\infty}\int_{-\infty}^{\infty} exp(p_x s_x^2 + q_x s_x) exp\left(p_y s_y^2 + q_y s_y\right) ds_x ds_y \end{aligned} \tag{10}$$

To solve Eq. (10), we benefit from 3.462.2 in [36] and the result yields

$$u_{r1}(r_x, r_y) = -\frac{\pi}{\sqrt{p_x p_y}} exp\left(\frac{{q_{x1}}^2}{4p_x} + \frac{{q_{y1}}^2}{4p_y}\right) exp\left(\frac{jkn_0^2}{2zn_e} {r_x}^2 + \frac{jkn_e}{2z} {r_y}^2\right) \tag{11}$$

Similarly, second part of the received field due to the second exponential function in source field is found using Eq. (12).

$$u_{r2}(r_x, r_y) = -\int_{-\infty}^{\infty}\int_{-\infty}^{\infty}\left(exp(as_x - bs_y) exp\left(-\frac{s_x^2 + s_y^2}{w^2}\right) exp\left(\frac{jk}{2zn_e}\left[\begin{array}{c} n_0^2(r_x^2 - 2r_x s_x + s_x^2) \\ +n_e^2(r_y^2 - 2r_y s_y + s_y^2) \end{array}\right]\right) ds_x ds_y\right) \tag{12}$$

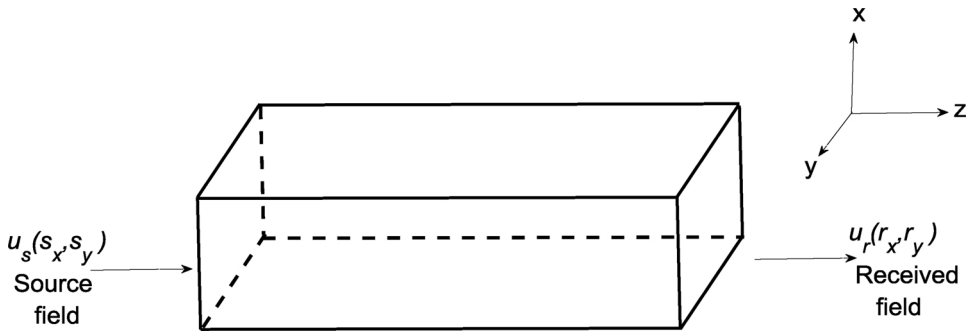

Fig. 1. View for the propagation in uniaxial crystal.

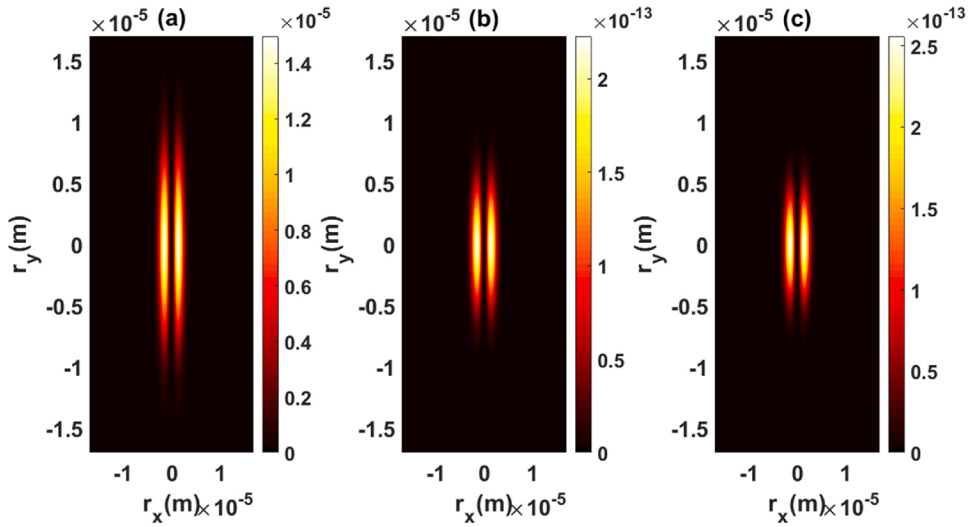

Fig. 2. Intensity profile of HSG beam having $a = b = 10^{-2}/w$, at $z = z_R$.

Likewise in evaluation of Eq. (10), we use the same integral in [36]. Result is found as

$$u_{r2}(r_x, r_y) = \frac{\pi}{\sqrt{p_x p_y}} exp\left(\frac{q_{x1}^2}{4p_x} + \frac{q_{y2}^2}{4p_y}\right) exp\left(\frac{jkn_0^2}{2zn_e} r_x^2 + \frac{jkn_e}{2z} r_y^2\right) \tag{13}$$

Similar with Eqs. (10) and (12) above, integral expression of third part of received field and its result, which is found applying the same approach in Eqs. (11) and (13), are given in Eqs. (14) and (15).

$$u_{r3}(r_x, r_y) = -\int_{-\infty}^{\infty}\int_{-\infty}^{\infty} \left(exp(-as_x + bs_y) exp\left(-\frac{s_x^2 + s_y^2}{w^2}\right) exp\left(\frac{jk}{2zn_e}\begin{bmatrix} n_0^2\left(r_x^2 - 2r_x s_x + s_x^2\right) \\ +n_e^2\left(r_y^2 - 2r_y s_y + s_y^2\right) \end{bmatrix}\right) ds_x ds_y \right) \tag{14}$$

$$u_{rx3}(r_x, r_y) = +\frac{\pi}{\sqrt{p_x p_y}} exp\left(\frac{q_{x2}{}^2}{4p_x} + \frac{q_{y1}{}^2}{4p_y}\right) exp\left(\frac{jkn_0^2}{2zn_e} r_x{}^2 + \frac{jkn_e}{2z} r_y{}^2\right) \tag{15}$$

Finally, the last part of received field is written as

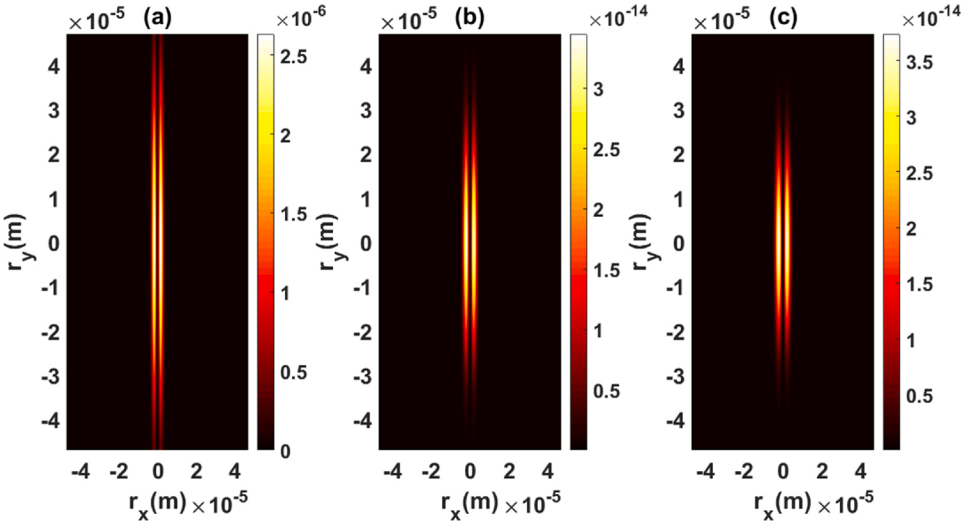

Fig. 3. Intensity profile of HSG beam having $a = b = 10^{-2}/w$, at $z = 5z_R$.

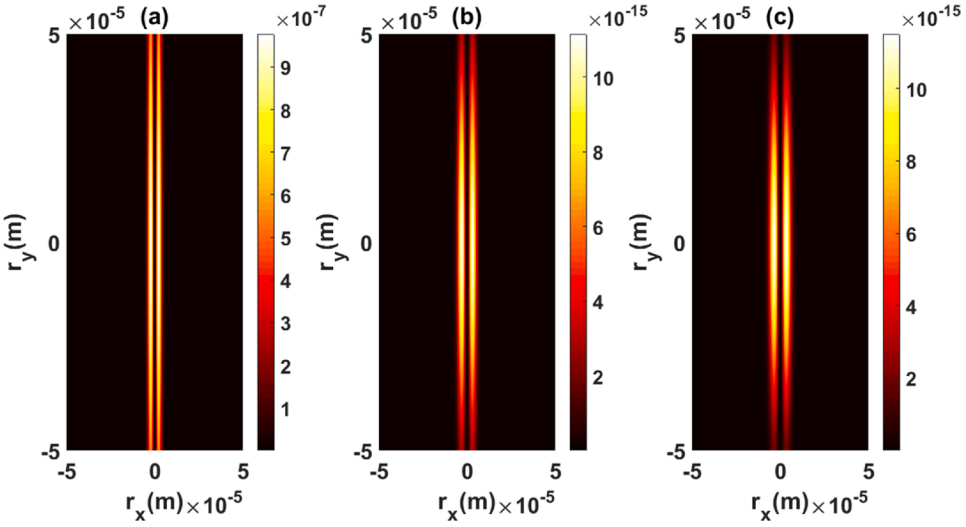

Fig. 4. Intensity profile of HSG beam having $a = b = 10^{-2}/w$, at $z = 10z_R$.

$$u_{r4}(r_x, r_y) = \int_{-\infty}^{\infty}\int_{-\infty}^{\infty}\left(exp(-as_x - bs_y)exp\left(-\frac{s_x^2+s_y^2}{w^2}\right)exp\left(\frac{jk}{2zn_e}\begin{bmatrix} n_0^2\left(r_x^2 - 2r_xs_x + s_x^2\right) \\ +n_e^2\left(r_y^2 - 2r_ys_y + s_y^2\right)\end{bmatrix}\right)ds_xds_y\right) \tag{16}$$

In a similar vein in evaluation of Eqs. (11), (13), and (15), results of Eq. (16) is found as

$$u_{r4}(r_x, r_y) = -\frac{\pi}{\sqrt{p_xp_y}}exp\left(\frac{{q_{x2}}^2}{4p_x} + \frac{{q_{y2}}^2}{4p_y}\right)exp\left(\frac{jkn_0^2}{2zn_e}{r_x}^2 + \frac{jkn_e}{2z}{r_y}^2\right) \tag{17}$$

Keeping in mind above calculations, received field of HSG beam in uniaxial crystal is written as

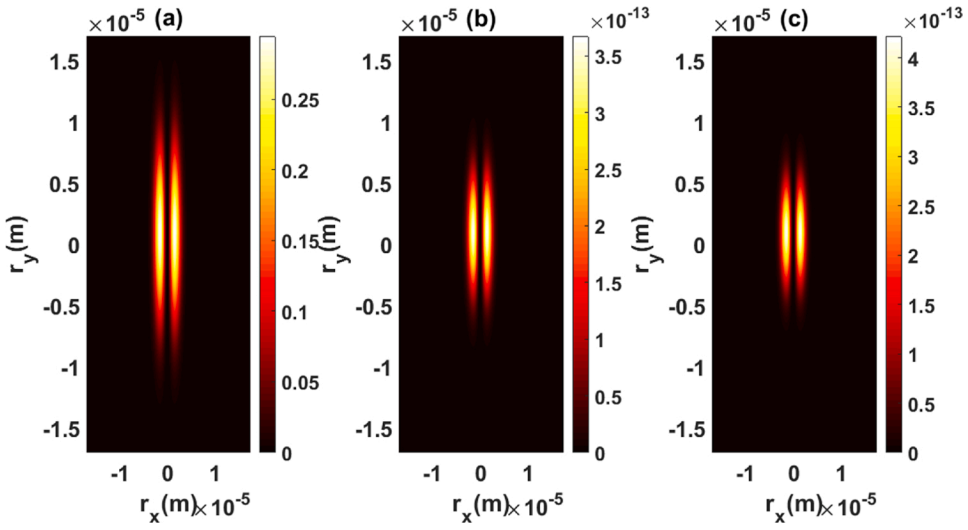

Fig. 5. Intensity profile of HSG beam having $a = b = 1/w$, at $z = z_R$.

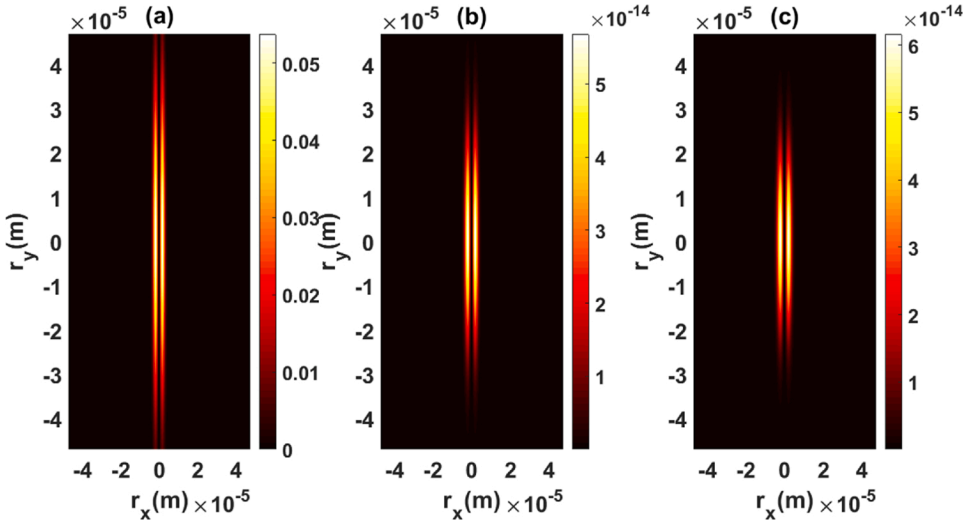

Fig. 6. Intensity profile of HSG beam having $a = b = 1/w$, at $z = 5z_R$.

$$u_r(r_x, r_y) = \frac{kn_0}{2\pi jz} exp(jkn_e z) \frac{\pi}{\sqrt{p_x p_y}} exp\left(\frac{jkn_0^2}{2zn_e} {r_x}^2 + \frac{jkn_e}{2z} {r_y}^2\right) \left\{ - exp\left(\frac{{q_{x1}}^2}{4p_x} + \frac{{q_{y1}}^2}{4p_y}\right) + exp\left(\frac{{q_{x1}}^2}{4p_x} + \frac{{q_{y2}}^2}{4p_y}\right) + exp\left(\frac{{q_{x2}}^2}{4p_x} + \frac{{q_{y1}}^2}{4p_y}\right) - exp\left(\frac{{q_{x2}}^2}{4p_x} + \frac{{q_{y2}}^2}{4p_y}\right) \right\} \tag{18}$$

3. Results and discussions

In this part of the study, we comment on the numerical results based on the evaluations in Section 2. In order to make comparison, we set $e = 1.1,\ 1.7,$ and 2 in subplots a, b, and c of each figure. Propagation distance is determined as $z = z_R,\ 5z_R,$ and $10z_R$ and Gaussian beam size w is equal to $2\mu m$. An example view for the propagation system is given in Fig. 1.

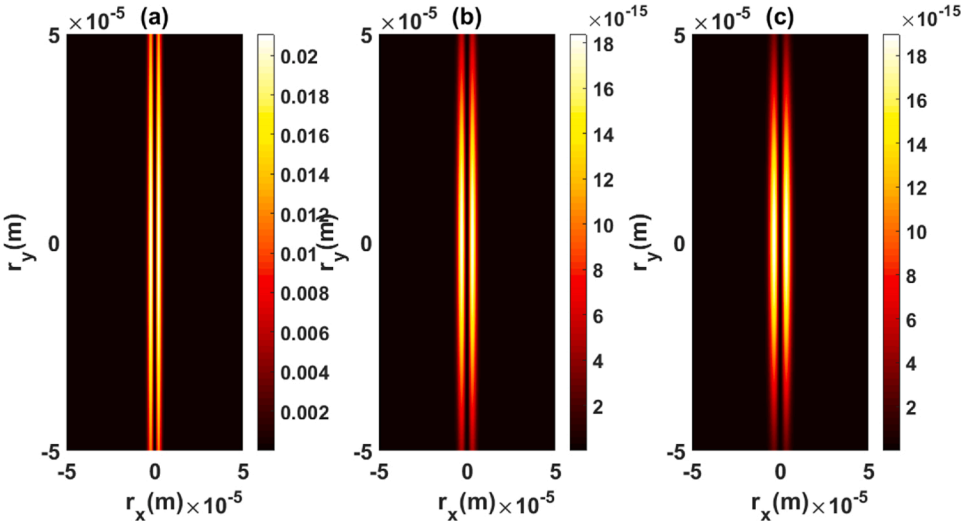

Fig. 7. Intensity profile of HSG beam having $a = b = 1/w$, at $z = 10z_R$.

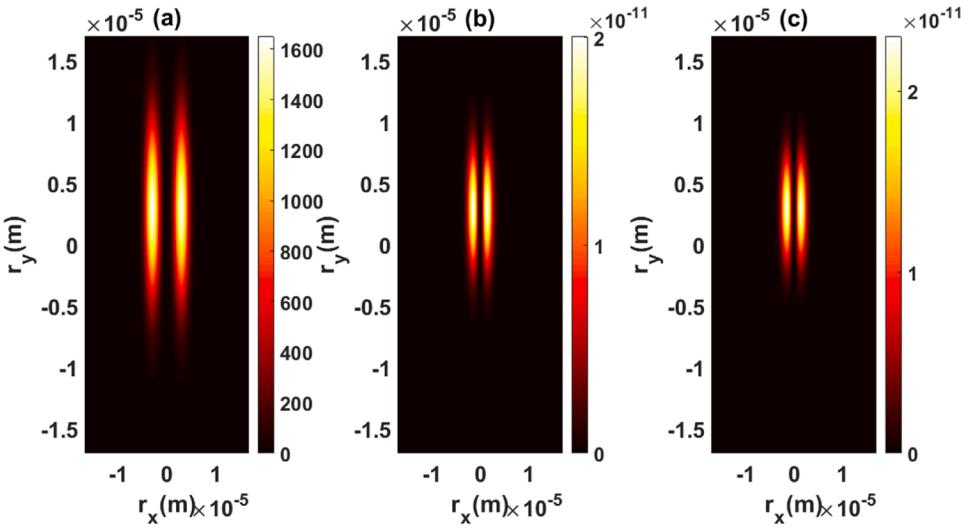

Fig. 8. Intensity profile of HSG beam having $a = b = 3/w$, at $z = z_R$.

To start with, Figs. 2–4 show intensity distribution of HSG beam at $z = z_R,\ 5z_R,$ and $10z_R$ when $a = b = 10^{-2}/w$. It is seen from these figures that intensity profile has two elliptic Gaussian lobes and ellipticity of beam raises while propagation distance increases, in other words from Fig. 2 up to 4, longer radius of elliptic shape lies along y axis. Generation of this elliptic distribution is because of the refractive index variations in crystal. Increase in propagation distance brings us reduction in peak intensity approximately amount of 10^{-1} and increase in beam size.

Effect of uniaxial crystal is observed by changing the value of e. At constant propagation distance, change in e from 1.1 to 1.7 and 2 reduces the peak intensity from 10^{-6} to 10^{-14} as it is observed from Fig. 3. In case of beam size, we observe smaller elliptic shape while e increases.

Next, source beam parameters are set to $a = b = 1/w$ in Figs. 5–7. We investigate from these figures that maximum intensity of

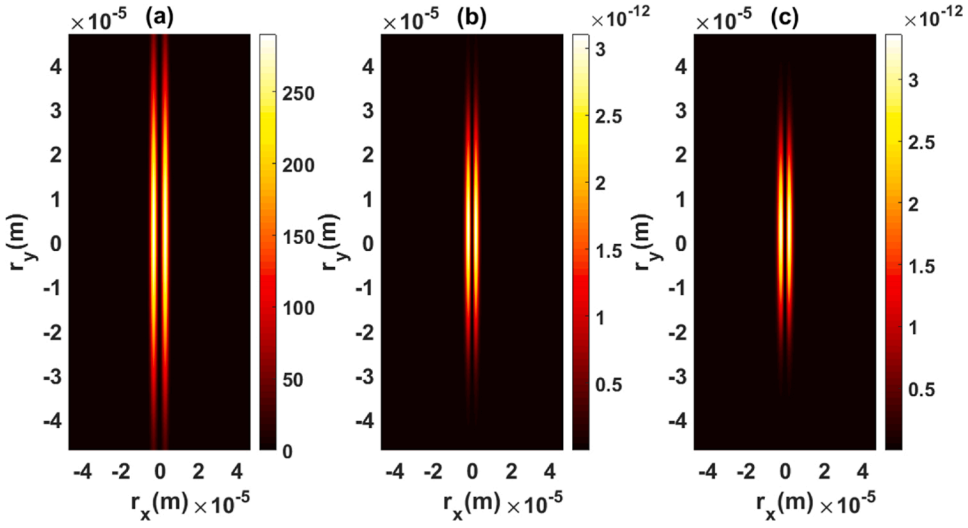

Fig. 9. Intensity profile of HSG beam having $a = b = 3/w$, at $z = 5z_R$.

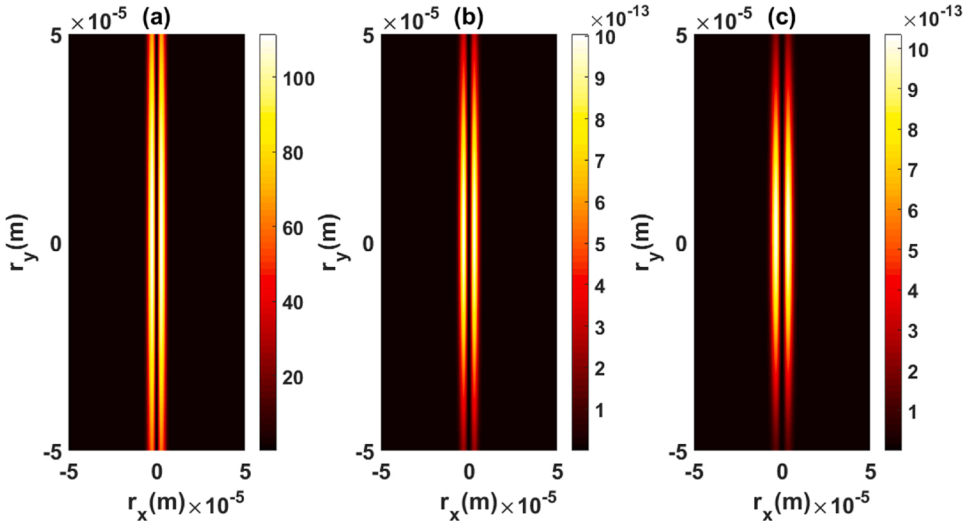

Fig. 10. Intensity profile of HSG beam having $a = b = 3/w$, at $z = 10z_R$.

beam decreases to its half when it is propagated by $5z_R$ as in Fig. 6. Here, critical point is the off-axis behavior of beam at close distance in Fig. 5.

This off-axis shape evolves into on-axis beam when propagation distance increases. Change in crystal settings or in other words changing the material of the crystal has an important influence on the peak intensity. Since different materials have different refractive index values, change in material will bring us change in extraordinary and ordinary refractive index ratio.

While peak intensity diminishes by 10^{-15} by scaling up refractive index ratio at close distance, it is seen that maximum intensity is lowered by 10^{-17} at longer distance in Fig. 7.

At Figs. 8–10, source beam parameters are determined as $a = b = 3/w$. First, off-axis distribution attracts the attention at $z = z_R$ as it is seen from Fig. 8. While e reduces, elliptic Gaussian lobes move away from each other. At 5 z_R distance, beam turns into on-axis shape as it is shown in Fig. 9.

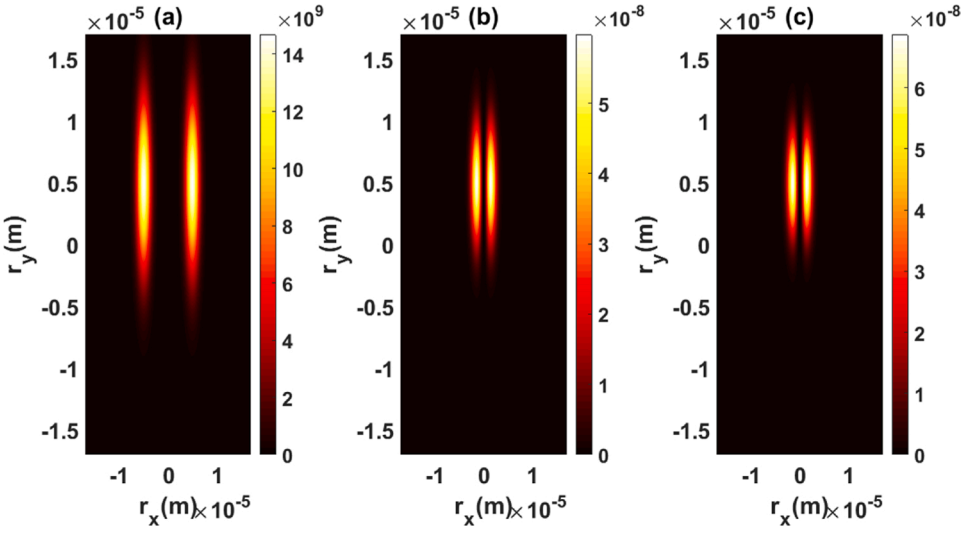

Fig. 11. Intensity profile of HSG beam having $a = b = 5/w$, at $z = z_R$.

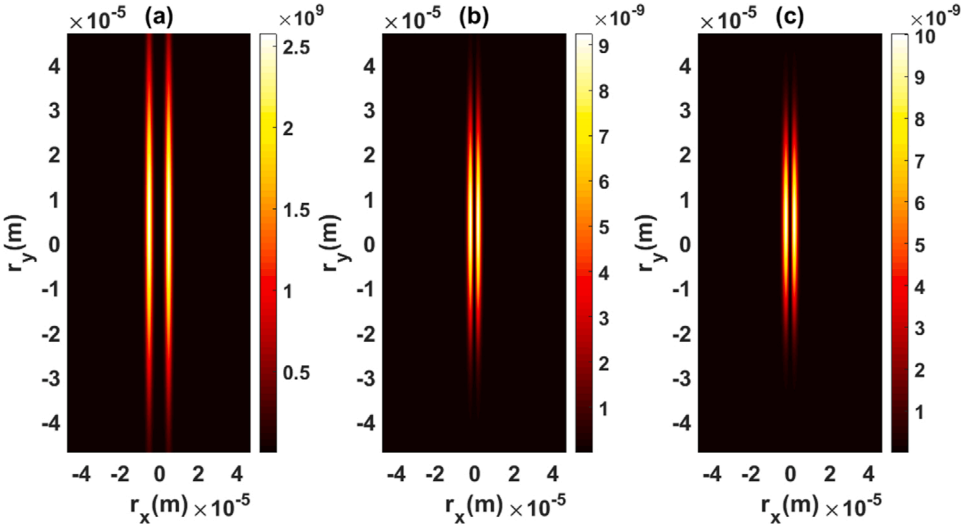

Fig. 12. Intensity profile of HSG beam having $a = b = 5/w$, at $z = 5z_R$.

Looking at Fig. 10, we understand that peak intensity mitigates by $1/10$ when beam is propagated by $10z_R$. Finally, source beam parameters are given as $a = b = 5/w$.

Off-axis intensity distribution is observed in Fig. 11 clearly at $z = z_R$. As propagation distance increases to $5z_R$ in Fig. 12, beam lies on on-axis by losing $1/10$ of peak intensity.

At $z = 10z_R$, beam size expands more and peak intensity does not decrease such amount of powers of 10 as it is showed in Fig. 13. Besides, maximum peak intensity is observed in this setting among all when $e = 1.1$. On the other hand, peak intensity decreases by 10^{-17} as refractive index ratio raises. It can be concluded as beam having less beam size have higher peak intensity as compared to other because power is constant in these conditions. In other saying, to satisfy the equal power, larger beam has lower peak intensity.

4. Conclusion

Received field expression of astigmatic hyperbolic sinusoidal Gaussian beam propagating through the uniaxial crystal orthogonal to the optical axis is derived analytically. Our results indicate that off-axis behavior at near field vanishes at far field and beam sits on on-axis. While propagation distance gets longer, peak intensity of beam decreases. Beam size at constant propagation distance can be controlled by setting crystal properties. Ordinary and extraordinary refractive index of crystal can be adjusted by selecting the crystal material like silica, quartz, and glass. It is possible to obtain more concentrated beam by increasing e. We assert that results of this study

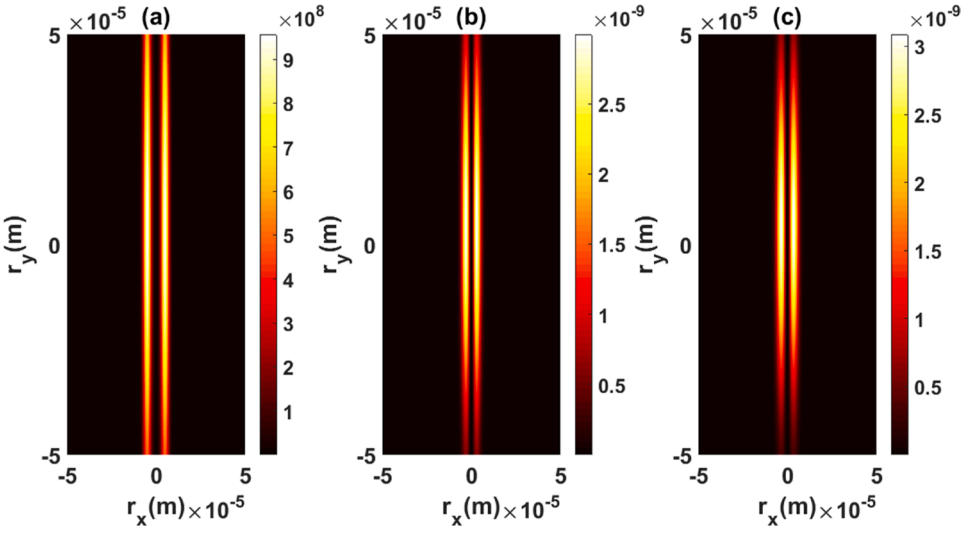

Fig. 13. Intensity profile of HSG beam having $a = b = 5/w$, at $z = 10z_R$.

will be beneficial for the applications based on optical tracking which is used to determine the position of the particles.

Declaration of Competing Interest

The authors report no declarations of interest.

References

[1] J. Lekner, Reflection and refraction by uniaxial crystals (in English), J. Phys.-Condens. Matter 3 (August (32)) (1991) 6121–6133.
[2] J. Lekner, Normal-incidence reflection and transmission by uniaxial crystals and crystal plates (in English), J. Phys.-Condens. Matter 4 (February (5)) (1992) 1387–1398.
[3] J. Lekner, Reflection ellipsometry of uniaxial crystals (in English), J. Opt. Soc. Am. A-Opt. Image Sci. Vis. 14 (June (6)) (1997) 1359–1362.
[4] J. Lekner, Optical-properties of an isotropic layer on a uniaxial crystal substrate (in English), J. Phys.-Condens. Matter 4 (August (31)) (1992) 6569–6586.
[5] J. Lekner, Optical properties of a uniaxial layer, Pure Appl. Opt. 3 (1994) 821.
[6] J. Lekner, Bounds and zeros in reflection and refraction by uniaxial crystals (in English), J. Phys.-Condens. Matter 4 (November (47)) (1992) 9459–9468.
[7] J. Lekner, Brewster angles in reflection by uniaxial crystals (in English), J. Opt. Soc. Am. A-Opt. Image Sci. Vis. 10 (September (9)) (1993) 2059–2064.
[8] J. Lekner, Reflection by uniaxial crystals: polarizing angle and Brewster angle (in English), J. Opt. Soc. Am. A-Opt. Image Sci. Vis. 16 (November (11)) (1999) 2763–2766.
[9] S.N. Kurilkina, V.N. Belyi, N.S. Kazak, Transformation of high-order Bessel vortices in one-dimensional photonic crystals (in English), J. Opt. 12 (January (1)) (2010).
[10] T.A. Fadeyeva, A.F. Rubass, I.S. Valkov, A.V. Volyar, Fractional optical vortices in a uniaxial crystal (in English), J. Opt. 15 (April (4)) (2013).
[11] G. Piquero, L. Monroy, M. Santarsiero, M. Alonzo, J.C.G. de Sande, Synthesis of full Poincare beams by means of uniaxial crystals (in English), J. Opt. 20 (June (6)) (2018).
[12] M.O. Ivanov, N.V. Shostka, Focusing of Gaussian beam passed under small angle to optical axis of uniaxial crystal (in English), J. Opt. 18 (July (7)) (2016).
[13] B. Gu, et al., Experimental investigation on the polarization evolution characteristics of arbitrary cylindrical vector beams in uniaxial crystals orthogonal to the optical axis (in English), Opt. Commun. 427 (November) (2018) 433–438.
[14] L. Jin, Dynamics of chirped finite Olver Gaussian beam propagating paraxial to uniaxial crystal (in English), Phys. Scr. 95 (March (3)) (2020).
[15] X.L. Ma, G.Q. Wang, H.Y. Zhong, A.Y. Dong, Y.C. Wang, D.J. Liu, Evolutions of random electromagnetic multi-Gaussian Schell-model vortex beams propagating in uniaxial crystals orthogonal to the optical axis (in English), Optik 203 (February) (2020).
[16] D.J. Liu, G.Q. Wang, H.Y. Zhong, H.M. Yin, A.Y. Dong, Y.C. Wang, Properties of a four-petal Lorentz-Gauss beam propagating in uniaxial crystal orthogonal to the optical axis (in English), Optik 183 (2019) 257–265.
[17] D.J. Liu, H.Y. Zhong, G.Q. Wang, H.M. Yin, Y.C. Wang, Evolution properties of a partially coherent Lorentz-Gauss vortex beam in a uniaxial crystal (in English), J. Mod. Opt. 66 (January (1)) (2019) 67–76.
[18] J. Li, Y.R. Chen, Propagation of confluent hypergeometric beam through uniaxial crystals orthogonal to the optical axis (in English), Opt. Laser Technol. 44 (July (5)) (2012) 1603–1610.
[19] X. Ma, G. Wang, H. Zhong, Y. Wang, D. Liu, Propagation of a rectangular multi-Gaussian Schell-model vortex beam in uniaxial crystal, Optik 221 (2020) 165318.
[20] D.J. Liu, H. Wang, Y.C. Wang, H.M. Yin, Propagation properties of elliptical Gaussian beam in uniaxial crystals along the optical axis (in English), Opt. Laser Technol. 73 (October) (2015) 12–18.
[21] O.F. Sayan, H. Gercekcioglu, Y. Baykal, Hermite Gaussian beam scintillations in weak atmospheric turbulence for aerial vehicle laser communications (in English), Opt. Commun. 458 (March) (2020).
[22] M.L. Zhou, C.D. Chen, B. Chen, X. Peng, Y.L. Peng, D.M. Deng, Propagation of an Airy-Gaussian beam in uniaxial crystals (in English), Chin. Phys. B 24 (December (12)) (2015).
[23] W.H. Yu, et al., Propagation of Airy Gaussian vortex beams in uniaxial crystals (in English), Chin. Phys. B 25 (April (4)) (2016).
[24] G.Q. Zhou, R.P. Chen, X.X. Chu, Propagation of cosh-Airy beams in uniaxial crystals orthogonal to the optical axis (in English), Opt. Laser Technol. 116 (August) (2019) 72–82.
[25] L. Li, et al., The effects of uniaxial crystal on off-axis hollow vortex Gaussian beams (in English), Optik 194 (October) (2019).
[26] C.J. Xu, et al., Propagation of a radially polarized Pearcey beam in uniaxial crystals (in English), Laser Phys. 28 (November (11)) (2018).

[27] C. Sun, X. Lv, D.M. Deng, B.B. Ma, H.Z. Liu, W.Y. Hong, Nonparaxial propagation of the radially polarized Airy-Gaussian beams with different initial launch angles in uniaxial crystals (in English), Opt. Commun. 445 (August) (2019) 147–154.
[28] D.D. Li, X. Peng, Y.L. Peng, L.P. Zhang, D.M. Deng, Nonparaxial evolution of the Airy-Gaussian vortex beam in uniaxial crystal (in English), J. Opt. Soc. Am. B-Opt. Phys. 34 (April (4)) (2017) 891–898.
[29] Y.H. Chen, L.X. Wu, Z.X. Mo, L.C. Wu, D.M. Deng, Nonparaxial propagation of radially polarized chirped Airy beams in uniaxial crystal orthogonal to the optical axis (in English), Chin. Phys. B 30 (January (1)) (2021).
[30] J.B. Zhang, K.Z. Zhou, J.H. Liang, Z.Y. Lai, X.L. Yang, D.M. Deng, Nonparaxial propagation of the Chirped Airy vortex beams in uniaxial crystal orthogonal to the optical axis (in English), Opt. Express 26 (January (2)) (2018) 1290–1304.
[31] J.R. Ye, J.B. Zhang, F. Ye, J.T. Xie, D.M. Deng, Propagation properties of the rotating elliptical chirped Gaussian beam in uniaxial crystals orthogonal to the optical axis (in English), Waves Random Complex Media (October) (2020).
[32] M. Bayraktar, Propagation of Airyprime beam in uniaxial crystal orthogonal to propagation axis, Optik 228 (2021) 166183.
[33] S. Shen, Z. Yang, J. Guo, Y. Wang, Z. Pang, Propagation characteristics of astigmatic hyperbolic sinusoidal Gaussian beams in nonlocal nonlinear media, Optik 224 (2020) 165454.
[34] M. Born, E. Wolf, Principles of Optics, 7th edn., Pergamon, Oxford, 1999.
[35] A. Yariv, P. Yeh, Optical Waves in Crystals, Wiley, New York, 1984.
[36] I.S. Gradshteyn, I.M. Ryzhik, Table of Integrals, Series, and Products, Academic Press, 2015, p. 1156.